

## **Bone cell-independent benefits of raloxifene on the skeleton: A novel mechanism for improving bone material properties**

Maxime A. Gallant<sup>1</sup>, Drew M. Brown<sup>1</sup>, Max Hammond<sup>2</sup>, Joseph M. Wallace<sup>3</sup>, Jiang Du<sup>4</sup>, Alix C. Deymier-Black<sup>5</sup>, Jonathan D. Almer<sup>6</sup>, Stuart R. Stock<sup>7</sup>, Matthew R. Allen<sup>1</sup>, David B. Burr<sup>1,3</sup>

<sup>1</sup>: Department of Anatomy & Cell Biology, Indiana University School of Medicine, 635 Barnhill Dr, MS-5035, Indianapolis, IN, 46202

<sup>2</sup>: Weldon School of Biomedical Engineering, Purdue University, 206 S. Martin Jischke Drive West Lafayette, IN 47907

<sup>3</sup>: Department of Biomedical Engineering, Indiana University-Purdue University at Indianapolis, 723 West Michigan Street, SL 220, Indianapolis, IN 46202

<sup>4</sup>: Department of Radiology, University of California, 200 West Arbor Drive, MC 0834 | San Diego, CA 92103

<sup>5</sup>: Department of Materials Science and Engineering, Northwestern University, 2220 Campus Drive, Cook Hall Room 2036, Evanston, IL 60208

<sup>6</sup>: Advanced Photon Source, Argonne National Laboratory, Building 401, 9700 S. Cass Avenue, Argonne, IL 60439

<sup>7</sup>: Department of Molecular Pharmacology and Biological Chemistry, Feinberg School of Medicine, Northwestern University, Abbott Hall Suite 810, 710 N Lake Shore Drive, Chicago IL 60611

Corresponding author: David B. Burr

Dept. of Anatomy and Cell Biology  
Indiana University School of Medicine  
635 Barnhill Dr, MS-5035  
Indianapolis, IN, 46202  
[dburr@iupui.edu](mailto:dburr@iupui.edu)

---

This is the authors' manuscript of the article published in final edited form as:

Gallant MA, Brown DM, Hammond M, Wallace JM, Du J, Deymier-Black AC, et al. Bone cell-independent benefits of raloxifene on the skeleton: A novel mechanism for improving bone material properties. *Bone*. 2014 Apr;61:191–200. Available from: <http://dx.doi.org/10.1016/j.bone.2014.01.009>

## **Abstract**

Raloxifene is an FDA approved agent used to treat bone loss and decrease fracture risk. In clinical trials and animal studies, raloxifene reduces fracture risk and improves bone mechanical properties, but the mechanisms of action remain unclear because these benefits occur largely independent of changes to bone mass. Using a novel experimental approach, machined bone beams, both from mature male canine and human male donors, were depleted of living cells and then exposed to raloxifene *ex vivo*. Our data show that *ex vivo* exposure of non-viable bone to raloxifene improves intrinsic toughness, both in canine and human cortical bone beams tested by 4-point bending. These effects are cell-independent and appear to be mediated by an increase in matrix bound water, assessed using basic gravimetric weighing and sophisticated ultrashort echo time magnetic resonance imaging. The hydroxyl groups (-OH) on raloxifene were shown to be important in both the water and toughness increases. Wide and small angle x-ray scattering patterns during 4-pt bending show that raloxifene alters the transfer of load between the collagen matrix and the mineral crystals, placing lower strains on the mineral, and allowing greater overall deformation prior to failure. Collectively, these findings provide a possible mechanistic explanation for the therapeutic effect of raloxifene and more importantly identify a cell-independent mechanism that can be utilized for novel pharmacological approaches for enhancing bone strength.

## **Keywords**

Raloxifene, mechanical testing, toughness, water

## **Abbreviations**

RAL: raloxifene, ALN: alendronate, RAL-4-Glu: raloxifene-4'-glucuronide, RAL bis-Me: raloxifene bismethyl ether

## **1. Introduction**

Skeletal fractures can occur when the loads imparted to the bone exceed its mechanical resistance. A bone's mechanical properties are determined by both its structure (mass, geometry, architecture) and the material properties of the tissue itself, such as mineral and collagen matrix composition, microdamage accumulation, collagen cross-linking, and tissue hydration [1]. Clinical strategies to reduce fracture risk have focused almost exclusively on improving bone mass, often assessed by bone mineral density (BMD). FDA approved anti-resorptive agents like bisphosphonates and denosumab significantly reduce fracture risk mainly by reducing osteoclast activity and bone turnover, thereby maintaining or elevating bone density by increasing mineralization [2]. Although increasing bone mass certainly improves bone's structural mechanical properties, changes in properties of the tissue itself can also significantly enhance bone's mechanical properties.

Raloxifene is a SERM (Selective Estrogen Receptor Modulator) used clinically in post-menopausal women to slow bone loss and decrease fracture risk [3]. Raloxifene suppresses osteoclast activity and bone remodeling in a manner similar to estrogen through high affinity interactions with ER $\alpha$  [4]. Compared to other anti-remodeling agents, such as bisphosphonates, raloxifene only modestly suppresses bone remodeling and induces little or no change in bone mineral density [5]. Despite small improvements in BMD, raloxifene significantly reduces vertebral fracture risk nearly as much as the bisphosphonates [6].

The mechanism for raloxifene's beneficial effects on bone has not been clearly elucidated, but our group has shown that raloxifene improves material-level mechanical (intrinsic) properties that are independent of bone mass and architecture [7-9]. These changes were most dramatic for bone toughness, a measure of the ability of the tissue to absorb energy prior to fracture. Following one year of treatment with clinically relevant doses of raloxifene in dogs, trabecular and cortical bone toughness in vertebrae, femoral neck and femoral diaphysis were twice those of vehicle-treated animals without a significant effect on bone volume or density [7, 8]. Despite these effects, both clinically and in the laboratory, the mechanisms responsible for enhancement of mechanical properties are unclear. The current work investigates the mechanisms involved in raloxifene's enhancement of bone toughness. We hypothesize that raloxifene acts directly on the bone matrix to improve material properties, specifically the modulus of toughness.

## **2. Material and methods**

### **2.1 Tissue, specimen processing and in vitro experiment**

Canine bone samples from treatment naïve animals were obtained through tissue sharing at Indiana University School of Medicine. Femora from skeletally mature (15-24 mo/old) female beagles (1 dog) and male hounds (8 dogs) were used. Animals were part of Institutional Animal Care and Use Committee approved protocols. Human bone samples (unembalmed tibial diaphysis; male, 87 and 51 years old, donor 1 and 2, respectively) were obtained through the Indiana University School of Medicine anatomical donation program. Prismatic beams (N= 8-12 beams per experimental group) were machined following the bone longitudinal axis using a low-speed saw fitted with a diamond-coated circular blade, and hand-sanded to 1.37 x 2 x 25 mm (Fig. 1a). Appropriate beam size was obtained using digital calipers ( $\pm 0.01$  mm) and measured at 5%, 33%, 66% and 95% of beam length. Beams were sonicated (30 sec) to remove debris and kept frozen in saline-soaked gauze until tested. All beams were subjected to freeze-thaw cycles (4-5 cycles) and a cell viability assay using lactase dehydrogenase (Suppl. Methods) showed no cellular survival after 1 freeze-thaw cycle (Fig. 1b). All incubations were performed in a 37°C humidified incubator in PBS (1X, 0.22  $\mu$ m filtered) supplemented with 1% penicillin-streptomycin. Because serum proteins can bind raloxifene, decreasing its relative binding affinity to ER $\alpha$  *in vivo* [10], fetal bovine serum (FBS) was used in one experiment to rule out this effect. Beams were incubated with specified compounds dissolved in dimethyl sulfoxide (DMSO) for 2 weeks at 2  $\mu$ M unless otherwise noted. DMSO is one of the best organic solvents and is required for raloxifene to enter into solution. Vehicle (DMSO) was kept constant in all groups at 0.04% vol/vol. The high (2  $\mu$ M) and low (5 nM) doses of raloxifene were chosen from the literature on the anti-oxidant effect of raloxifene, which spans from the low micromolar to the millimolar range [11-14], and its activation of the estrogen receptor, usually accomplished with low nanomolar concentration respectively [15, 16]. The low dose is also in the same range as the reported  $C_{max}$  (maximum effective concentration) of raloxifene (EVISTA product label, Eli Lilly). The alendronate dose used was equal on a molar basis to the high RAL dose (2  $\mu$ M), while 17 $\beta$ -Estradiol was used at 0.5  $\mu$ M, a dose shown to exert anti-oxidant effects [11, 17].

## 2.2 Mechanical testing

Beams were subjected to 4-point bending on a 100P225 modular test machine (TestResources) with a 150 lb force transducer using a custom support with a lower span set at 12 mm and upper span at 4 mm (Fig. 1a). Beams were loaded to fracture at 2 mm/min, and displacement measured at 15 Hz from the actuator. We did not account for test frame compliance and although we recognize that this can affect the absolute measurements, it is not expected to alter the relative effects described in this paper. Structural variables recorded included ultimate load (F), stiffness (S), and energy to failure (U). Yield

point was determined as 0.2% offset from the linear portion of the loading curve. Ultimate stress ( $\sigma_{ult}$ ), modulus (E), and toughness (u) were estimated using standard equations for four-point bending of beam specimens:  $\sigma_{ult} = F * (3L / 2wt^2)$ ,  $E = (S/wt^3) \times (6La^2) - 8a^3$ ,  $u = 9U/(wt(3L - 4a))$ , where L is the span of the lower fixture, a is half of the difference between the lower and upper fixture span, and w and t are the specimen width and height (Fig. 1a) [7]. Following testing, the pieces of bone were wrapped in saline-soaked gauze and frozen.

### 2.3 Gravimetric Analysis of Water Content

Pieces of previously broken beams were thawed and re-hydrated in PBS (or PBS+other compounds) for 2 days. Specimens were then patted dry, weighed (wet weight) and dried in a 100°C oven. Weights were recorded every 24h until stable for 2 consecutive days (3 to 4 days total). Bone density of PBS and RAL-treated samples (Suppl. Table 1) were obtained using wet weight and uCT-derived bone volume, and used to convert the lost water weight into volumetric percent of lost water. Water density was set at 1 mg/mm<sup>3</sup>.

### 2.4 3D Ultrashort Echo Time Magnetic Resonance Imaging (UTE MRI)

The bone samples were stacked and placed in a 3 ml syringe filled with perfluorooctyl bromide (PFOB) solution to minimize susceptibility effects and enhance tissue-air contrast. A three-dimensional (3D) ultrashort echo time (UTE) sequence was implemented on a 3T Signa TwinSpeed scanner (GE Healthcare Technologies, Milwaukee, WI) which had a maximum gradient strength of 40 mT/m and a maximum slew rate of 150 mT/m/ms. The 3D UTE sequence employed a short rectangular pulse (duration = 32  $\mu$ s) for non-slice selective excitation followed by 3D radial ramp sampling with a nominal TE of 8  $\mu$ s. The regular 3D UTE sequence was used to image both the short and long  $T_2$  water [18, 19]. The shorter  $T_2$  water components were selectively imaged with 3D inversion recovery (IR) prepared UTE sequence, where a relatively long adiabatic inversion pulse (8.6 ms in duration) was employed to simultaneously invert and suppress long  $T_2$  water signal [20]. A home-made 1-inch diameter birdcage transmit/receive (T/R) coil was used for signal excitation and reception. Typical imaging parameters included a TR of 300 ms, a flip angle of 10°, sampling bandwidth of 125 kHz, imaging field of view (FOV) of 8 cm, reconstruction matrix of 256×256×256. For IR-UTE imaging, a TI of 90 ms was used for long  $T_2$  free water suppression [18].

Total bone water volume percent concentration was quantified by comparison of 3D UTE image signal intensity from the bone with that from an external reference standard [20, 21]. The reference

standard was distilled water doped with  $\text{MnCl}_2$  to reduce its  $T_2^*$  to close to that of cortical bone ( $\sim 400$   $\mu\text{s}$ ). The reference tube was placed close to the bone samples and both were near the coil isocenter. Variation in coil sensitivity was corrected by dividing the 3D UTE signal from bone or the reference phantom by the 3D UTE signal obtained from a separate scan of a 20 ml syringe filled with distilled water. Relaxation during RF excitation was ignored since the rectangular pulse was significantly shorter than both the  $T_1$  and  $T_2^*$  of cortical bone.  $T_1$  effects were ignored since the long TR of 300 ms guaranteed virtually full recovery of longitudinal magnetization of bone ( $T_1$  of around 200 ms at 3T) and reference phantom ( $T_1$  of around 5 ms) when using a low flip angle of  $10^\circ$  [22].  $T_2$  effects could also be ignored because the UTE sequence had a nominal TE of 8  $\mu\text{s}$  and the  $T_2^*$  of the water phantom was close to that of bone. Bound water concentration was measured by comparing the 3D IR-UTE signal intensity of cortical bone with that of the water calibration phantom. Errors due to coil sensitivity, as well as  $T_1$  and  $T_2^*$  effects were corrected in a similar way.

### *2.5 Atomic Force Microscopy (AFM)*

A non-damaged portion of each canine bone beam was polished using a 3  $\mu\text{m}$  polycrystalline water-based diamond suspension (Buehler LTD; Lake Bluff, IL). To remove extrafibrillar surface mineral and expose underlying collagen fibrils, each beam was treated with 0.5M EDTA at a pH of 8.0 for 20 minutes followed by sonication for 5 minutes in water. This process was repeated 4 times.

Samples were imaged using a Bruker Catalyst AFM in peak force tapping mode. Images were acquired from 4-5 locations in each beam using a silicon probe and cantilever (RTESPA, tip radius = 8 nm, force constant 40 N/m, resonance frequency 300 kHz; Bruker) at line scan rates of 0.5 Hz at 512 lines per frame in air. Peak force error images were analyzed to investigate the D-periodic spacing of individual collagen fibrils. At each location, 5-15 fibrils were analyzed in 3.5  $\mu\text{m}$  x 3.5  $\mu\text{m}$  images (approximately 70 total fibrils in each of 4 samples per group). Following image capture, a rectangular region of interest (ROI) was chosen along straight segments of individual fibrils. A two dimensional Fast Fourier Transform (2D FFT) was performed on the ROI and the primary peak from the 2D power spectrum was analyzed to determine the value of the D-periodic spacing for that fibril (SPIP v5.1.5, Image Metrology; Hørsholm, Denmark).

### *2.6 Wide and Small Angle X-ray Scattering (WAXS and SAXS, respectively)*

Beams of canine bone treated with raloxifene or PBS were examined using high-energy x-ray scattering at Sector 1 of the Advance Photon Source (APS) at Argonne National Laboratory (Argonne, IL).

The samples were mounted into the 4-point bend attachment of a servo-hydraulic MTS-858 load frame and kept wet throughout the test (phosphate buffered saline was periodically applied to each beam). The samples were placed in the attachment so that their 2.0 and 1.4 mm dimensions were perpendicular and parallel to the loading direction, respectively. The spacing between the upper support dowels was 6 mm while that of the lower dowels varied between 16 mm for sample RLX1 and 14 mm for all of the other samples. Decreasing the lower span decreases per unit applied force, the rate at which stress rises on the outside of the bar, and assured that a sufficient number of data points could be collected before fracture. The samples were deformed in increments of 20  $\mu\text{m}$  crosshead displacement as measured by the load frame, which resulted in a load increase of  $\sim 5\text{-}10$  N in the linear elastic region. The applied load was measured by a 1 kN load cell attached to the load frame; its precision is 0.1% of the rated maximum load and fluctuations no larger than 1-2 N were observed during the course of data collection. Stable and proportionate rises in measured load were observed with crosshead deflections of 2  $\mu\text{m}$  and below. A linear variable displacement transducer, located inside the MTS actuator, was used to monitor crosshead displacement, with an estimated resolution of 2  $\mu\text{m}$ . At each displacement increment, 20 x-ray scattering measurements, spaced 100  $\mu\text{m}$  apart, were made across the sample in the loading direction, of which only  $\sim 12$  actually passed through the sample. After each series of 20 positions, the load frame was translated laterally by 100  $\mu\text{m}$  to minimize x-ray dose accumulation. The resolution of the vertical translations (sample and MTS load frame) is better than 1  $\mu\text{m}$ . Note that the start of each series of WAXS/SAXS measurements was also offset vertically from the previous scan by an amount roughly equal to the crosshead displacement increment.

The measurements were made with a 50 x 50  $\mu\text{m}$  monochromatic x-ray beam (70 keV energy) that traversed the sample perpendicular to the loading direction. The WAXS patterns were measured with an x-ray detector placed 2,081.8 mm from the sample in order to obtain HAP 00.2 diffraction rings. The detector consisted of 4 GE-41RT flat panel detectors (2,048 x 2,048 pixels, 200 x 200  $\mu\text{m}^2/\text{pixel}$ ), arranged in a flower-shaped pattern about the transmitted beam. Each detector was rotated in the anti-clockwise direction at an angle of 37° with respect to its horizontal direction. The SAXS patterns were collected simultaneously with the WAXS patterns, through an opening in the WAXS detector array. The SAXS detector (PI-CCD detector, 1,000 x 1,000 pixels, 22.5  $\mu\text{m}/\text{pixel}$ ) was  $\sim 4$  m from the specimen.

Using ceria diffraction patterns (pressed  $\text{CeO}_2$  powder disk, NIST SRM-674a), accurate values of sample-to-detector distance, detector tilt, and beam center were measured for each WAXS detector using the program Fit2D. These values were then input into a series of custom-made programs written in MatLab at the APS. These programs convert the diffraction patterns from radial to Cartesian

coordinates and fit the shape of the peak of interest, HAP 00.2, with a pseudo-Voigt function. The peak center is taken to be the center of the fitted peak. To obtain the longitudinal d-spacing, the HAP(00.2) radial peak center was determined for detector azimuthal angular ranges of  $0\pm 20^\circ$  and  $180\pm 20^\circ$ , orientations associated with HAP platelets that have their c-axis aligned with the long axis of the sample beams, and converted to d-spacing according to Bragg's law. Note that the beams had such great crystallographic texture that diffracted intensities outside these ranges were too low for accurate fitting. The d-spacings at  $0\pm 20^\circ$  and  $180\pm 20^\circ$  were averaged to obtain the longitudinal HAP d-spacing. These d-spacings were then converted to HAP phase strains using the following equation:  $\epsilon_{\text{HAP}} = (d - d_0) / d_0$ , where  $\epsilon_{\text{HAP}}$  is the HAP longitudinal strain,  $d$  is the d-spacing at the load of interest, and  $d_0$  is the d-spacing at zero load. For narrow diffraction peaks using this approach, WAXS derived strains can typically be measured to  $\sim 1 \times 10^{-4}$  but for bone (wide diffraction peaks) this value might be as large as  $3 \times 10^{-4}$ . The phase strains were then plotted as a function of position in the sample and as a function of local applied load. The local applied load was converted to local applied stress using the equation:  $\sigma = 3Plz / 2wh^3$  where  $P$  is the applied load in N,  $l$  is the span between the outer support points,  $z$  is the location on the sample in the direction of loading ( $z=0$  at the sample center),  $w$  is the width of the sample and  $h$  is the height of the sample. The slope of plots of HAP strain vs. local stress is the apparent modulus which provides information about load transfer between the HAP and the collagen in bone.

The separation between the SAXS detector and specimen was refined using a 7200 line/mm Au-coated grating (SLG-C72-121A-Au from LightSmyth). The collagen D-period ( $\sim 67$  nm) produced measurable first and third order peaks in the SAXS regime. These peaks were fit and the results analyzed in the same way as the HAP 00.2. The mineralized collagen fibril strains were computed from  $\epsilon_{\text{fibril}} = (D - D_0) / D$ , where  $\epsilon_{\text{fibril}}$  is the fibril longitudinal strain,  $D$  is the D-period at the load of interest, and  $D_0$  is the D-period at zero load.

## 2.7 Statistical analyses

Data are presented as means  $\pm$  SEM, unless otherwise stated. Statistical analyses were performed using GraphPad Prism v5.04 (GraphPad Software, San Diego, CA). T-tests were used to compare 2 groups together, one-way ANOVAs followed by *Bonferroni post-hoc* tests were used for multiple group comparisons and 2-way ANOVAs were used for the human donors. A paired t-test was used for BMC measurements pre- and post-incubation. To investigate differences in fibril morphology distributions, a Kolmogorov-Smirnov test was performed on the cumulative distribution function from each group. For all tests, a value of  $p < 0.05$  was considered significant.



### 3. Results

#### 3.1 Raloxifene improves material-level mechanical properties through cell-independent actions

Incubation of bone beams in RAL for 2 wks resulted in a concentration-dependent improvement in bone tissue toughness (Fig. 2a), with the high concentration (2  $\mu$ M) of RAL producing a 103% higher toughness, and the lower concentration (5 nM) a 53% increase, compared to the vehicle control (PBS [PBS plus 0.04% (vol/vol) of DMSO]). Because of its maximal effect, the high concentration was used in subsequent experiments. The addition of 5% fetal bovine serum did not diminish raloxifene's positive effect on toughness (Fig. 2b).

Consistent with canine bone, RAL significantly improved human bone tissue toughness by an average of 22% (Fig. 2c). These effects were not due to mineral matrix dissolution during the incubation as there was no change in bone mineral content (Fig. 2d, and Suppl. Methods). Furthermore, a combination of microCT and RAMAN spectroscopy analyses showed no difference in canine bone volume, porosity or composition after the two week incubation period in either PBS or raloxifene (Suppl. Table 1).

The mechanical effects of raloxifene were expressed predominantly by a change in the post-yield properties. The greater energy to failure (+34%) in the canine raloxifene beams was due to higher post-yield energy (+38%) as no change was seen in the energy to yield when compared to PBS-treated beams (Fig. 2e,f). Ultimate stress, a material strength index, was modestly higher with raloxifene exposure (+9.8%), but only in the canine specimens, whereas modulus did not differ in either canine or human experiments (Suppl. Table 2). These results are consistent with animal studies that show raloxifene treatment has minimal effects on pre-yield energy absorption while significantly increasing post-yield energy absorption [7].

To determine if the positive mechanical effects of raloxifene occur quickly or require extended exposure to the drug, and to determine whether withdrawal of the raloxifene results in a return to pre-treatment mechanical properties, beams were exposed to RAL for 2 days, followed by incubation in PBS for an additional 12 days. Tissue toughness was similar in specimens exposed to RAL for 2 days and 2 wks, and both were significantly higher than control specimens (Fig. 2g).

#### 3.2 Hydroxyl groups contribute to the enhanced mechanical properties with raloxifene

Structurally, raloxifene contains two hydroxyl groups (-OH, positions 4' and 6) on the 2-arylbenzothiophene core of the molecule (Fig. 3a, boxed area). The partially inactive raloxifene-4'-

glucuronide (RAL-4-Glu), a glucuronidated liver metabolite of raloxifene [23], and raloxifene bismethyl ether (RAL bis-Me), an estrogen receptor inactive compound on which both hydroxyl groups are absent [16], were tested to determine whether they affect bone tissue properties in the *ex vivo* beam model. After 2 weeks of incubation, RAL-4-Glu had 19% higher toughness compared to control (PBS), but this was significantly less than the 36% enhancement in tissue toughness induced by RAL (Fig. 3b). RAL bis-Me had no effect on tissue toughness, suggesting a role of the 2 hydroxyl groups of raloxifene in modifying bone tissue toughness.

Chemically, the arylbenzothiophene core structure of raloxifene (Fig 3a, boxed area) resembles that of estrogen, and the hydroxyl groups on 17 $\beta$ -estradiol are 11Å apart, while the 4' and 6-OH groups of raloxifene are 11.3Å apart (MM2 analysis, ChemBio3D Ultra v.12.0.2). Therefore, 17 $\beta$ -estradiol (17 $\beta$ -E2, 0.5  $\mu$ M) was tested. Following two wks of incubation with 17 $\beta$ -E2, bone beams had 31% greater toughness than control (Fig. 3b), and were not significantly different from RAL. As a control, alendronate (ALN, 2  $\mu$ M), a commonly used bisphosphonate in treatment of osteoporosis, was tested and did not affect toughness compared to control beams after 2 wks of exposure (Fig 3b).

### 3.3 Raloxifene alters strains transferred to HAP

To investigate the mechanisms of the increase in material toughening, synchrotron x-ray scattering during 4 pt-bending was performed, and the WAXS and SAXS patterns of PBS and RAL-treated beams were analyzed. This technique allows quantification of the strains experienced by the hydroxyapatite (HAP) crystal and mineralized collagen fibrils under bending [24]. Each series of 20 WAXS/SAXS patterns was shifted vertically (along the loading direction) from the previous scan by an amount equal to the change in crosshead displacement. Transitions between no sample scattering and strong WAXS and SAXS patterns and between no sample absorption and significant sample absorption were observed at the expected vertical positions and confirmed that the crosshead displacements accurately reflected deflections of the specimens.

Moduli were calculated for each of the different increases in loading during the WAXS and SAXS testing, which led to about 10-15 values per sample. Statistical analyses of these values from the stress-strain curves revealed that the HAP apparent moduli, the ratio of local applied stress to local phase strain, were higher for the RAL beams compared to PBS (averages of 24.4 $\pm$ 7.5 and 32.5 $\pm$ 12.1 GPa for RAL and 23.2 $\pm$ 7.0 and 26.8 $\pm$ 9.2 GPa for PBS beams,  $p < 0.05$  for RAL over PBS). Fibril strains tracked HAP strains linearly. The macroscopic fracture mode of the samples examined with WAXS/SAXS (MTS load frame) was assumed to be similar to those of the specimens tested with the Test Resources system.

Figure 4 shows the magnitude of the HAP longitudinal strain as a function of position across the specimen for each of 12 (Fig. 4a, PBS-treated) or 14 (Fig. 4b, raloxifene-treated) crosshead displacements before sample failure. The magnitudes of the HAP longitudinal strains were larger in the PBS beam, while the RAL sample was able to accommodate much larger displacements before failure. In the PBS beam, the HAP longitudinal tensile curves (bottom half of the specimen) ran linear to the edge of the specimen at lower applied displacements and became bilinear at larger crosshead displacements (Fig. 4a), indicating yielding. In the compressive portion of the PBS beam, the curves also became bilinear but at higher crosshead displacements than in the tensile portion of the specimen. In the RAL sample, the HAP tensile longitudinal strains plateaued first in the lower portion of the sample and the compressive HAP longitudinal strains later in upper portions of the specimen. Moreover, the RAL-treated beam continued to deform and the longitudinal HAP strains changed dramatically post-yield (Fig. 4b, dashed lines): over most of the beam thickness, the HAP longitudinal strains became compressive and higher than those preceding the yield point. Plots of fibril longitudinal strain for each position and each applied displacement show precisely the same behavior as Fig. 4a and b and are not shown.

Two points are important in interpreting the data of Fig. 4b. First, the diffraction-derived (HAP and fibril) strains reflect changes in d-spacing (D-period) and essentially reflect stored elastic energy. Second, HAP (fibril) strain will drop to zero if the specimen cracks significantly in the volume sampled or if the applied load is removed (cracking elsewhere leading to local unloading). Therefore, as long as the HAP (fibril) strains remain significant, regardless of the sign, the specimen is carrying load in the sampled volume. Examined in this light, Fig. 4b shows an applied displacement of 200  $\mu\text{m}$  produces yielding only in the specimen's bottom two positions have yielded (those in greatest tension, about 100  $\mu\text{m}$  into the specimen); yielding here means the HAP longitudinal strains reach and maintain a maximum strain of  $\sim 3 \times 10^{-3}$ . After a displacement of 360  $\mu\text{m}$ , in the tensile portions of the specimen, seven positions (about 600  $\mu\text{m}$  into the specimen) have yielded. Up to this displacement, the compressive side of the specimen shows only elastic behavior (linear HAP longitudinal strain vs position). At 400  $\mu\text{m}$  displacement, the spatial distribution of HAP longitudinal strains transitions: a much larger fraction of the sample contains the maximum compressive HAP strains ( $> -3 \times 10^{-3}$ ,  $\sim 500 \mu\text{m}$  into the specimen) and a greatly decreased portion of the specimen ( $\sim 100 \mu\text{m}$  from the specimen edge) contains the large tensile strains. The HAP data for RAL, therefore, show the sample remains mechanically competent (still carrying loads) up to 560  $\mu\text{m}$  displacement although there are clear indications of incipient failure in the waviness of the

strain vs position curve. Upon increasing the displacement beyond 560  $\mu\text{m}$ , load could no longer be maintained and the sample macroscopically failed.

### 3.4 Raloxifene increases matrix-bound water and modifies collagen nanomorphology

Raloxifene significantly increased cortical bone water content by 17% over PBS-treated beams, (Fig. 5a) independent of porosity and density (Suppl. Table 1). Water content was significantly correlated to toughness (Fig. 5b), more specifically to post-yield toughness (Table 1), in the RAL-treated canine beams but not in PBS-only specimens. Ultimate stress and modulus were negatively correlated with water content in the RAL-treated beams. To test whether increased water level by RAL is retained following *in vivo* exposure to the drug, tissue from dogs treated daily for 1 year with clinically relevant doses of raloxifene was further analyzed. Previous work from these animals demonstrated significantly higher bone toughness compared to placebo-treated animals [7]. Water content was also higher in raloxifene-treated dogs compared to the vehicle-treated dogs (+5% over VEH, Fig. 5c), and was positively correlated with tissue toughness, whereas no relationship was observed in the vehicle-treated dogs (Fig. 5d). These results suggest that *in vivo* treatment with raloxifene also alters bone hydration measured *ex vivo*, which correlated to increased tissue toughness.

Interestingly, water content was negatively correlated to energy to yield in both the PBS and the RAL groups (Table 1 and Fig. 5e). There was no difference between the two slopes ( $p = 0.09$ ), but the intercepts were different ( $p < 0.001$ ), indicating that the relationship between water content and energy absorption is different up to the yield point. Conversely, the post-yield and total energy to failure both positively correlated with water content, but only in the RAL group (Fig. 5f-g). Water content was also analyzed in beams treated with the raloxifene metabolites. RAL-4-Glu increased water content (+8.1% over PBS) to a level intermediate between RAL and PBS, while RAL bis-Me ether had no effect on water content (Fig. 5h), consistent with the effects of these compounds on tissue toughness (Fig. 3b). These results suggest that the increased bone water content and increased toughness associated with raloxifene treatment may be mediated by the two hydroxyl groups of the molecule. Estradiol increased water content by 16.7% over PBS beams, while ALN had no effect on hydration (Fig. 5h). In the human samples, RAL increased water content by 7% and 8.6% in donor 1 and 2, respectively (Fig. 5i), and the increases correlated with the increases in toughness in both donors ( $r^2$ : 0.59,  $p = 0.0001$ , Suppl. Table 3).

PBS and RAL treated beams were subjected to 3D UTE MRI [19] to determine whether the increase in water occurred in the free or bound water compartments. Total and bound water were significantly increased (+17% for total and +20% for bound water over PBS) in the RAL-treated beams

compared to the PBS beams (Fig. 5j), but free water was not significantly different (+10% over PBS,  $p=0.23$ ). This suggests that raloxifene is either chemically or physically modifying the bone matrix thus increasing the bound water fraction. Both total water and bound water fraction from UTE MRI correlated with tissue toughness and post-yield toughness, while no correlation was observed for the free water compartment (Table 2). Consistent with the gravimetric analyses, the PBS-soaked beams had no relationship with water content calculated from 3D UTE MRI.

To understand if collagen fibril morphology was altered by raloxifene, fibrillar D-periodic spacing was assessed using atomic force microscopy. The mean D-periodic spacing was not different in the RAL beams compared to the PBS beams (Fig. 6a,  $p=0.126$ ), but the range of D-periodic spacing was widened by RAL exposure. The distribution of the collagen fibril D-periodic spacing was shifted significantly to higher values in the raloxifene group compared to the control beams (Fig. 6b).

#### **4. Discussion**

This study shows that a pharmacologic agent that reduces osteoporotic fracture risk while providing only a modest increase in bone mass can improve bone mechanical and material properties through a novel, cell-independent mechanism. It has been thought that the only pharmacological way to reduce fracture risk with age was to augment bone mass or slow its decay. Although this hypothesis is still valid, the quality and material properties of the bone tissue also play important roles in fracture prevention. Previous studies conducted by our group have shown that raloxifene improves bone material properties independently of bone mass in animal models [7, 8] [9]. These observations combined with the clinical fracture risk reduction [3] led to our hypothesis that raloxifene might exert some of its actions in a novel way, by acting on bone matrix. The absence of viable cells in these specimens of this study suggests that raloxifene imparts these effects by a direct physical effect on the bone matrix, rather than through a cell-mediated mechanism. This is consistent with a recent study that showed that *ex vivo* exposure of rat bone to strontium chloride increased bone stiffness and toughness, and that this effect was greatest in bone from ovariectomized rats [25].

Bone tissue toughness was our primary material property outcome as it represents the ability of the tissue to absorb energy and resist fracture, and represents a parameter associated with bone quality. The increase in material toughness by raloxifene appears related to the presence of two hydroxyl groups on the molecule. Interestingly, estradiol also significantly enhanced bone material toughness, suggesting that these observed effects are not specific to raloxifene, but are more generalizable to compounds with similar structures, most notably in the hydroxyl moieties. As shown before, the hydroxyl groups on 17 $\beta$ -

estradiol and raloxifene are almost equidistant from each other (11Å and 11.3Å, respectively). These hydroxyl groups are highly reactive due to the high electron density of the hydroxyl oxygen atom and are likely to form hydrogen bonds with different substrates, suggesting that both compounds could interact similarly with bone tissue matrix. In addition, it opens the possibility that endogenous estrogen, or estrogen replacement therapy, both known to reduce the risk of fracture, could be acting mechanistically in part through this non-cell mediated pathway. Conversely, the bisphosphonate alendronate, also known to reduce fractures, had no effect on tissue toughness or water content. This is consistent with a recent publication showing that alendronate decreases bone water content *in vivo* [26], but this is secondary to an increase in mineralization or lower porosity, parameters not changed in the present study. Our data also show that RAL acts at a lower dosage (5 nM) than the one used in this study (2 µM). Whether or not raloxifene increases material toughness at lower concentrations, whether it does it in a linear fashion or not or upon a longer exposure than the ones currently used remains unknown.

The present study investigated different avenues to explain the increase in toughness at the molecular level. It was found that RAL-treated samples had higher modulus values, obtained by WAXS and SAXS, suggesting that in these samples, RAL alters transfer of load between the collagen matrix and the HAP crystals, placing lower strains on the HAP, and points to the possibility that the collagen and mineral (HAP) interface is modified in the RAL samples. This is based on only two samples, which does not account for potential inter-sample or inter-individual variation, but the experimental data nevertheless represent 2,000 scattering patterns. Although our interpretation, of these data needs to be buttressed by increasing the number of treated and control specimens studied by WAXS/SAXS during *in situ* loading, the WAXS/SAXS data can be considered a preliminary proof-of-principle. If RAL modifies the collagen-HAP interface, weakening interfacial bonding and decreasing load transfer, this would increase the HAP apparent modulus. Modeling work by Luo *et al* [27], suggests that a weaker interface containing water would result in more diffuse damage within mineralized biomaterials, which could explain the increased energy absorption. We hypothesize that the increase in water by RAL at the interface between collagen and mineral allows slipping in that plane, prolonging the period of post-yield deformation. This concept is further supported by data from the longitudinal HAP and fibril strains, i.e., the strains in the HAP crystals with c-axes perpendicular to the loading direction showing that these strains were larger in the PBS samples compared to the RAL beam with the same also being true of the collagen phase and its strains. Based on these observations, it is possible that raloxifene is physically enabling the structure to bear these strains without failing by modifying the collagen-matrix interface.

Recent studies [28, 29] have demonstrated that D-spacing in normal collagen exists not with a singular value but with a distribution of values in a variety of tissues. Both estrogen depletion [28] and a defined genetic alteration in the *col1 $\alpha$ 1* gene [29] significantly altered this distribution in bone. This characteristic of collagen may provide important information about the internal structure or state of individual tropocollagen molecules, post-translational modifications occurring during collagen formation and/or enzymatic and non-enzymatic cross-linking. How changes in D-spacing are linked to altered mechanics is not fully understood. However, changes with raloxifene treatment, particularly increased D-spacing values, suggest the possibility of swelling within the fibrillar structure could be caused by increased water content.

Water plays an important role in bone mechanics, exemplified by experiments in which dry bone has higher strength and lower toughness compared to hydrated bone [30, 31]. Previous work has shown a strong negative relationship with respect to hydration and toughness [31, 32] using dehydrated bone as a model. In human bone, both bound water and toughness decrease with age [32-35]. Within bone, a small fraction of water exists in 'free' form in the Haversian canals, osteocyte lacunae and canaliculi. A larger fraction of bone water exists in 'bound' form, either tightly bound to the crystals of the apatite-like mineral and collagen molecules or loosely bound to the organic matrix. These two water compartments have been linked to different mechanical and material properties of bone tissue [35, 36]. Ultrashort echo time (UTE) magnetic resonance imaging (MRI) sequences with nominal echo times (TEs) less than 100  $\mu$ s have been developed to image and quantify water within cortical bone [20, 21] and can differentiate between "free" and "bound" water compartments within bone [20, 32, 36]. Our results showing a positive relationship between bound water and toughness are in agreement with existing literature. Bae *et al.* [35] showed that bound water positively correlated with failure energy in osteoporotic bone beams while Nyman *et al.* [32] showed that bound water and toughness were both decreased with age in cadaveric tissue. *In vitro* sequential dehydration of cortical bone beams has also been shown to be correlated to a reduced work to fracture [31], indicating a positive impact of hydration on bone biomechanics. The present study shows that raloxifene directly affects hydration of the bone matrix, specifically the water fraction that is bound to collagen and/or mineral and this water compartment has been postulated to provide the post-yield toughness of bone tissue [31], which is a parameter increased by raloxifene on our study. Although both PBS and RAL treatments showed intra-group variation in the amount of water present, RAL treatment increased it significantly and only the RAL-treated beams showed a correlation between volumetric water and material toughness. An explanation for the intra-group difference might be that the extent to which water can be bound

depends on a number of factors, which might include the bone mineral content in that region, or the extent to which the collagen is cross-linked. However, our RAMAN experiments did not detect any of these changes.

The hydroxyl groups on the raloxifene molecules seem important for the increase in toughness and water shown in these experiments. These reactive groups have been shown to be important for the molecule's binding to the ER $\alpha$  receptor, and their removal greatly diminishes the binding capacity of raloxifene [16]. Our results with estradiol and raloxifene-4-glucuronide suggest that not only the presence of hydroxyl groups, but their spatial position and orientation are important: estradiol has 2 hydroxyl groups in a position similar to those of raloxifene, while the glucuronidated metabolite has 5 hydroxyl groups, but does not increase tissue toughness or water content as much as raloxifene or estradiol.

It is unknown if clinical use of raloxifene or estrogen-like compounds in the treatment of osteoporosis increase bone water in humans. However, our group has previously shown that *in vivo* raloxifene treatment increases bone toughness in dogs [7], and we show now that this is associated with increased bone water. There is evidence that postmenopausal women have increased total body water when treated with raloxifene [37], which raises the possibility that bone hydration might be increased. Moreover, there is evidence that with age, human bone water decreases along with material toughness [32]. Also, we showed the same relationship between toughness and water in canine and human bone samples, thus suggesting that one can expect our *in vivo* and *ex vivo* dog results to be translatable to humans. The effects of RAL on the human samples are less dramatic than those on the canine bones, although they show the same patterns. This can be due to species-specific differences in bone composition, but are likely to be an age-related response. Specimens from older aged people may be less capable of increasing and sequestering water between collagen and mineral than bone from younger animals or people. However, within the human age range studied in this work (ages 51-87 years old), although both water content (Figure 5I) and toughness (Figure 2C) were less in the older subject, the response in water content and toughness upon exposure to raloxifene was about the same, indicating either a minor effect or no effect of age on the response of bone to raloxifene with the age-range of interest for the treatment of osteoporosis.

It is therefore possible that raloxifene counteracts both water and toughness decreases in postmenopausal osteoporotic women, possibly by altering the nanomorphology of the collagen fibril and the collagen-mineral interface, which in return reduces the fracture risk in this population.



## **5. Conclusion**

The importance of the present study is that it shows for the first time that the relationship between hydration and bone mechanics holds true when hydration is increased, and most importantly, that hydration can be positively affected through pharmaceutical treatment. It further demonstrates that raloxifene positively affects tissue-level biomechanical properties of bone through non-cell mediated effects on hydration. These results could open avenues to engineering of new compounds that do not act through cellular processes, but specifically target the mineral and collagen interface to increase hydration and energy absorption and reduce fracture risk of bone.

## **6. Acknowledgements**

The authors would like to thank Dr. Paul K. Hansma (Department of Physics, University of California, Santa Barbara), for suggesting the soaking technique and Dr. John Okasinski, Advanced Photon Source, for helping collect the WAXS data. Raloxifene was kindly provided by Eli Lilly (Indianapolis, IN, USA) under a Material Transfer Agreement to D.B.B. Eli Lilly was not involved in the study design, analyses or interpretation of the results. We are grateful to Dr. Susan J. Gunst for sharing dog tissue. Use of the Advanced Photon Source was supported by the US Department of Energy, Office of Science, Office of Basic Energy Sciences, under Contract No. DE-AC02-06CH11357. This work was supported by NIH grants to D.B.B. and M.R.A.

## REFERENCES

- [1] Felsenberg D, Boonen S. The bone quality framework: determinants of bone strength and their interrelationships, and implications for osteoporosis management. *Clinical therapeutics* 2005;27: 1-11.
- [2] Baron R, Ferrari S, Russell RGG. Denosumab and bisphosphonates: different mechanisms of action and effects. *Bone* 2011;48: 677-692.
- [3] Ettinger B, Black DM, Mitlak BH, Knickerbocker RK, Nickelsen T, Genant HK, Christiansen C, Delmas PD, Zanchetta JR, Stakkestad J, Gluer CC, Krueger K, Cohen FJ, Eckert S, Ensrud KE, Avioli LV, Lips P, Cummings SR. Reduction of vertebral fracture risk in postmenopausal women with osteoporosis treated with raloxifene: results from a 3-year randomized clinical trial. Multiple Outcomes of Raloxifene Evaluation (MORE) Investigators. *JAMA* 1999;282: 637-45.
- [4] Bryant HU. Mechanism of Action and Preclinical Profile of Raloxifene, a Selective Estrogen Receptor Modulator\*. *Reviews in Endocrine and Metabolic Disorders* 2001;2: 129-138.
- [5] Gallagher JC, Levine JP. Preventing osteoporosis in symptomatic postmenopausal women. *Menopause* 2011;18: 109-118.
- [6] Reginster J-Y. Antifracture efficacy of currently available therapies for postmenopausal osteoporosis. *Drugs* 2011;71: 65-78.
- [7] Allen MR, Hogan HA, Hobbs WA, Koivuniemi AS, Koivuniemi MC, Burr DB. Raloxifene enhances material- level mechanical properties of femoral cortical and trabecular bone. *Endocrinology* 2007;148: 3908-3913.
- [8] Allen MR, Iwata K, Sato M, Burr DB. Raloxifene enhances vertebral mechanical properties independent of bone density. *Bone* 2006;39: 1130-1135.
- [9] Diab T, Wang J, Reienwald S, Guldberg RE, Burr DB. Effects of the Combination Treatment 1 of Raloxifene and Alendronate on the Biomechanical Properties of Vertebral Bone. *J Bone Miner Res* 2010;26: 270-276.
- [10] Wijayaratne AL, Nagel SC, Paige LA, Christensen DJ, Norris JD, Fowlkes DM, McDonnell DP. Comparative analyses of mechanistic differences among antiestrogens. *Endocrinology* 1999;140: 5828-5840.
- [11] Mann V, Huber C, Kogianni G, Collins F, Noble B. The antioxidant effect of estrogen and Selective Estrogen Receptor Modulators in the inhibition of osteocyte apoptosis< i> in vitro</i>. *Bone* 2007;40: 674-684.
- [12] Arteaga E, Villaseca P, Bianchi M, Rojas A, Marshall G. Raloxifene is a better antioxidant of low-density lipoprotein than estradiol or tamoxifen in postmenopausal women in vitro. *Menopause* 2003;10: 142-146.
- [13] Yu J, Eto M, Kozaki K, Akishita M, Okabe T, Ouchi Y. Raloxifene analogue LY117018 suppresses oxidative stress-induced endothelial cell apoptosis through activation of ERK1/2 signaling pathway. *European journal of pharmacology* 2008;589: 32-36.
- [14] Blasbichler M, Arakil-Aghajanian A, Sinzinger H. Raloxifene does not prevent fibrinogen oxidation in vitro. *Medical science monitor: international medical journal of experimental and clinical research* 2005;11: PI1.
- [15] Krum SA, Miranda-Carboni GA, Hauschka PV, Carroll JS, Lane TF, Freedman LP, Brown M. Estrogen protects bone by inducing Fas ligand in osteoblasts to regulate osteoclast survival. *The EMBO journal* 2008;27: 535-545.
- [16] Grese TA, Cho S, Finley DR, Godfrey AG, Jones CD, Lugar CW, Martin MJ, Matsumoto K, Pennington LD, Winter MA. Structure-activity relationships of selective estrogen receptor modulators: modifications to the 2-arylbenzothiophene core of raloxifene. *Journal of medicinal chemistry* 1997;40: 146-167.

- [17] Lu A, Frink M, Choudhry MA, Hubbard WJ, Rue LW, Bland KI, Chaudry IH. Mitochondria play an important role in 17 $\beta$ -estradiol attenuation of H<sub>2</sub>O<sub>2</sub>-induced rat endothelial cell apoptosis. *American Journal of Physiology-Endocrinology And Metabolism* 2007;292: E585-E593.
- [18] Horch RA, Gochberg DF, Nyman JS, Does MD. Clinically compatible MRI strategies for discriminating bound and pore water in cortical bone. *Magnetic Resonance in Medicine* 2012;68: 1774-1784.
- [19] Du J, Bydder M, Takahashi AM, Carl M, Chung CB, Bydder GM. Short T2 contrast with three-dimensional ultrashort echo time imaging. *Magnetic resonance imaging* 2011;29: 470-482.
- [20] Du J, Carl M, Bydder M, Takahashi A, Chung CB, Bydder GM. Qualitative and quantitative ultrashort echo time (UTE) imaging of cortical bone. *Journal of Magnetic Resonance* 2010;207: 304-311.
- [21] Techawiboonwong A, Song HK, Leonard MB, Wehrli FW. Cortical Bone Water: In Vivo Quantification with Ultrashort Echo-Time MR Imaging<sup>1</sup>. *Radiology* 2008;248: 824-833.
- [22] Du J, Hamilton G, Takahashi A, Bydder M, Chung CB. Ultrashort echo time spectroscopic imaging (UTESI) of cortical bone. *Magnetic Resonance in Medicine* 2007;58: 1001-1009.
- [23] Kemp DC, Fan PW, Stevens JC. Characterization of raloxifene glucuronidation in vitro: contribution of intestinal metabolism to presystemic clearance. *Drug metabolism and disposition* 2002;30: 694-700.
- [24] Almer J, Stock S. Micromechanical response of mineral and collagen phases in bone. *Journal of structural biology* 2007;157: 365-370.
- [25] Cattani-Lorente M, Rizzoli R, Ammann P. In vitro exposure to strontium improves bone material level properties. *Acta Biomater* 2013;9: 7005-7013.
- [26] Anumula S, Wehrli SL, Magland J, Wright AC, Wehrli FW. Ultra-short echo-time MRI detects changes in bone mineralization and water content in OVX rat bone in response to alendronate treatment. *Bone* 2010;46: 1391-1399.
- [27] Luo Q, Nakade R, Dong X, Rong Q, Wang X. Effect of mineral–collagen interfacial behavior on the microdamage progression in bone using a probabilistic cohesive finite element model. *Journal of the mechanical behavior of biomedical materials* 2011;4: 943-952.
- [28] Wallace JM, Erickson B, Les CM, Orr BG, Banaszak Holl MM. Distribution of type I collagen morphologies in bone: Relation to estrogen depletion. *Bone* 2010;46: 1349-1354.
- [29] Wallace JM, Orr BG, Marini JC, Holl MMB. Nanoscale morphology of Type I collagen is altered in the Brl mouse model of Osteogenesis Imperfecta. *Journal of structural biology* 2011;173: 146-152.
- [30] Yan J, Daga A, Kumar R, Mecholsky JJ. Fracture toughness and work of fracture of hydrated, dehydrated, and ashed bovine bone. *Journal of biomechanics* 2008;41: 1929-1936.
- [31] Nyman JS, Roy A, Shen X, Acuna RL, Tyler JH, Wang X. The influence of water removal on the strength and toughness of cortical bone. *Journal of biomechanics* 2006;39: 931-938.
- [32] Nyman JS, Ni Q, Nicoletta DP, Wang X. Measurements of mobile and bound water by nuclear magnetic resonance correlate with mechanical properties of bone. *Bone* 2008;42: 193-199.
- [33] Wang X, Shen X, Li X, Mauli Agrawal C. Age-related changes in the collagen network and toughness of bone. *Bone* 2002;31: 1-7.
- [34] Zioupos P, Currey J. Changes in the stiffness, strength, and toughness of human cortical bone with age. *Bone* 1998;22: 57-66.
- [35] Bae WC, Chen PC, Chung CB, Masuda K, D'Lima D, Du J. Quantitative ultrashort echo time (UTE) MRI of human cortical bone: correlation with porosity and biomechanical properties. *Journal of Bone and Mineral Research* 2012;27: 848-857.
- [36] Horch RA, Gochberg DF, Nyman JS, Does MD. Non-invasive predictors of human cortical bone mechanical properties: T2-discriminated 1H NMR compared with high resolution X-ray. *PloS one* 2011;6: e16359.

[37] Jacobsen DE, Samson MM, Emmelot-Vonk MH, Verhaar HJ. Raloxifene and body composition and muscle strength in postmenopausal women: a randomized, double-blind, placebo-controlled trial. *European Journal of Endocrinology* 2010;162: 371-376.

## FIGURE LEGENDS

**Fig. 1.** (a) Schematic of the mechanical testing setup and beam dimensions. (b) Lactate dehydrogenase immunostaining of fresh (i) and frozen-thawed (ii) bone. Blue staining indicates living bone cells (osteocytes) in the bone matrix. Previously frozen-thawed bone (1 freeze-thaw cycle) shows no living cells.

**Fig. 2.** Raloxifene increases toughness in canine and human bone. (a) Raloxifene increases canine cortical bone toughness in a dose-dependent fashion after 2 wks of incubation (RAL-L: 5 nM, RAL-H: 2  $\mu$ M). (b) Addition of 5% serum (fetal bovine, FBS) does not prevent raloxifene (2  $\mu$ M), from increasing bone material toughness in our model. (c) Toughness is increased by raloxifene (2  $\mu$ M), in human bone beams from two different donors. (d) No change in BMC was observed between groups pre- and post-incubation. (e) Raloxifene (2  $\mu$ M), increases energy absorption in canine bone in the post-yield portion of the mechanical testing curve. Panel (f) represents the average force-displacement curves obtained from the high raloxifene dose in dogs (Fig. 2a) and in human donor 2 (Fig. 2c). (g) Toughness is increased in beams treated with raloxifene for 2 days then PBS for 12 days without raloxifene. This increase was not significantly different from the increase from 14 days of exposure to raloxifene ( $\beta = 0.60$  to detect a difference at  $\alpha = 0.05$ ;  $n = 8$  beams/group). \*:  $p < 0.05$ , \*\*:  $p < 0.01$ , \*\*\*:  $p < 0.001$  compared to PBS, a:  $p < 0.05$ , #:  $p < 0.05$  compared to FBS.  $N = 8-12$  beams/group.

**Fig. 3.** Raloxifene metabolites show reduced effect on material toughness. (a) Structures of the chemical compounds used in the study. Note the hydroxyl groups on carbons 4' and 6 of the arylbenzothiophene core (boxed) of raloxifene: These groups are successively removed on raloxifene-4'-glucuronide (RAL-4-G) and raloxifene bismethyl ether (RAL bis-Me). (b) Incubation of canine cortical beams in RAL-4-G (2  $\mu$ M) showed an abrogated increase in material toughness compared to raloxifene (2  $\mu$ M), while RAL bis-Me (2  $\mu$ M), showed no effect on material toughness. 17 $\beta$ -Estradiol (17 $\beta$ -E<sub>2</sub>; 0.5  $\mu$ M) also increased material toughness after 2 weeks of incubation and was not different from RAL. Alendronate (ALN, 2  $\mu$ M), a non-estrogenic compound used in the treatment of bone disease, showed no effect on tissue toughness. \*:  $p < 0.05$ , \*\*:  $p < 0.01$ , \*\*\*:  $p < 0.001$  compared to PBS, a:  $p < 0.05$ , b:  $p < 0.01$  compared to RAL, ‡:  $p < 0.05$  compared to RAL-4-G.  $N = 8-12$  beams/group.

**Fig. 4.** Raloxifene alters strains transferred to HAP. Graphs represent the longitudinal HAP strain of a PBS (a) and RAL-treated beam (b) relative to the position tested on the beam (x-axis, position 1: top of the

beam, position 20: bottom of the beam, see Suppl. Fig. 1) under increasing displacement. Filled lines represent pre-yield curves, dashed lines are post-yield and dashed black lines represent testing at the fracture load. Negative strains indicate compressive behavior, while positive strains are tensile. To simplify the plots, every other applied displacement is shown.

**Fig. 5.** Raloxifene increases water content in cortical canine bone. (a) Beams treated with RAL showed increased water content compared to PBS control beams (N=14-16 beams/group). (b) Water content from the RAL group shows positive correlation with tissue toughness, while no correlation is seen for the control beams. (c) Water content is higher in bone samples of dogs treated for 1 year with raloxifene (RAL, 0.5 mg/kg/day) compared to vehicle-treated dogs (VEH, saline, 1ml/kg/d, n=7 beams/group) and this correlates with bone material toughness (panel (d), toughness from [7])). (e) There was no difference between the two slopes ( $p = 0.09$ ), but the intercepts were different ( $p < 0.0001$ ), indicating that the relationship between water content and energy absorption are different up to the yield point. The relationship between water and total energy to failure (g) as well as with energy absorption in just the post-yield part of the load-deformation curve (f) are positive, while no relationship is present for the PBS controls (f,g). (h) Water content was lower in the RAL-4-G-treated beams compared to the RAL beams, while RAL bismethyl ether did not change water content compared to control beams.  $17\beta$ -Estradiol significantly increased water content to the same level as RAL, while ALN had no effect on that parameter (n = 8-12 beams/group). (i) Water was significantly increased in the human beam samples (both donors, n = 10 for each donor). (j) Bound water fraction measured by 3D UTE MRI in beams from canine bone is increased by raloxifene. Both total and bound water fractions were increased in raloxifene-treated cortical beams, while no difference was observed in the free water fraction. (N=8-10 beams/group). \*:  $p < 0.05$ , \*\*\*:  $p < 0.001$  compared to PBS, \*\*:  $p < 0.01$  compared to VEH, a:  $p < 0.05$ , b:  $p < 0.01$  compared to RAL.

**Fig. 6.** Raloxifene modifies collagen D-periodic spacing in cortical beams. (a) Raloxifene-treated beams showed no difference in mean or median D-periodic spacing compared to control beams, but had a significant shift in the population distribution towards more fibers with increased D-spacing (b). Boxplots represent the 25<sup>th</sup> and 75<sup>th</sup> percentiles, median line, min and max values and diamonds represent the mean for the groups. N=4 beams for each group, 207-222 fibrils/group.

Figure 1. Gallant et al, 2013

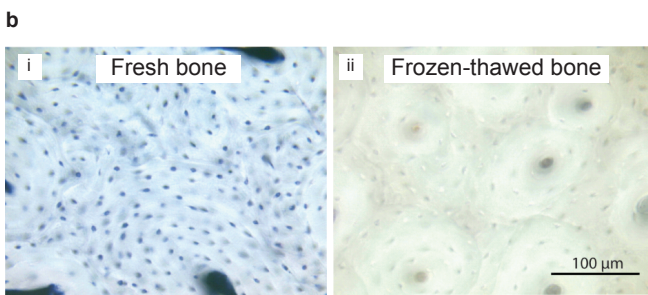
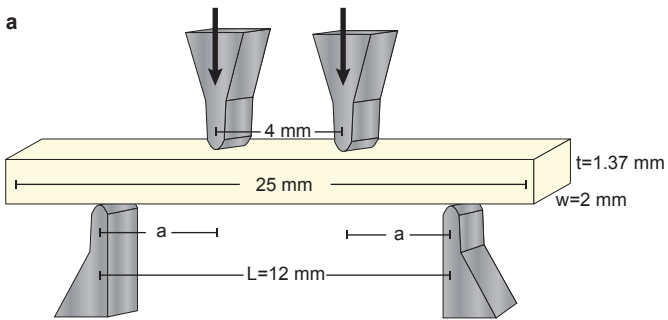


Figure 2. Gallant et al, 2013

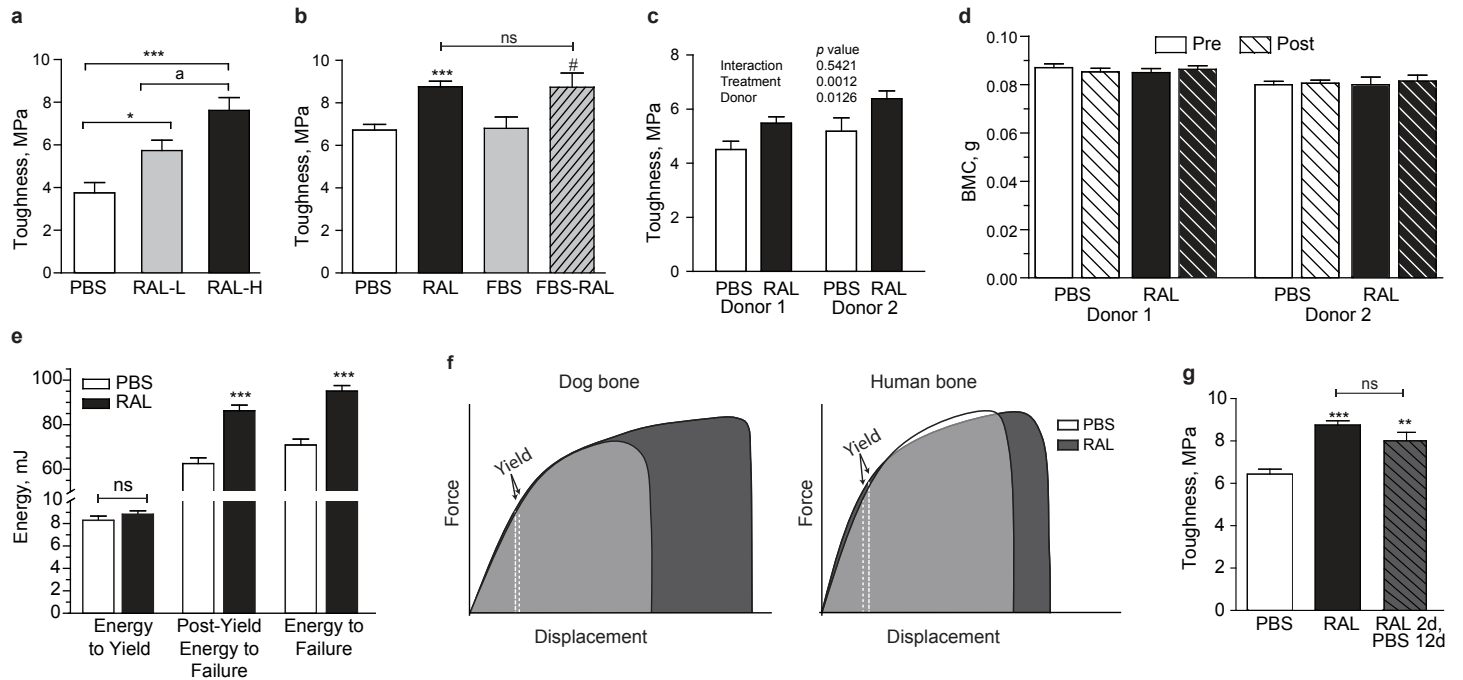




Figure 3. Gallant et al, 2013

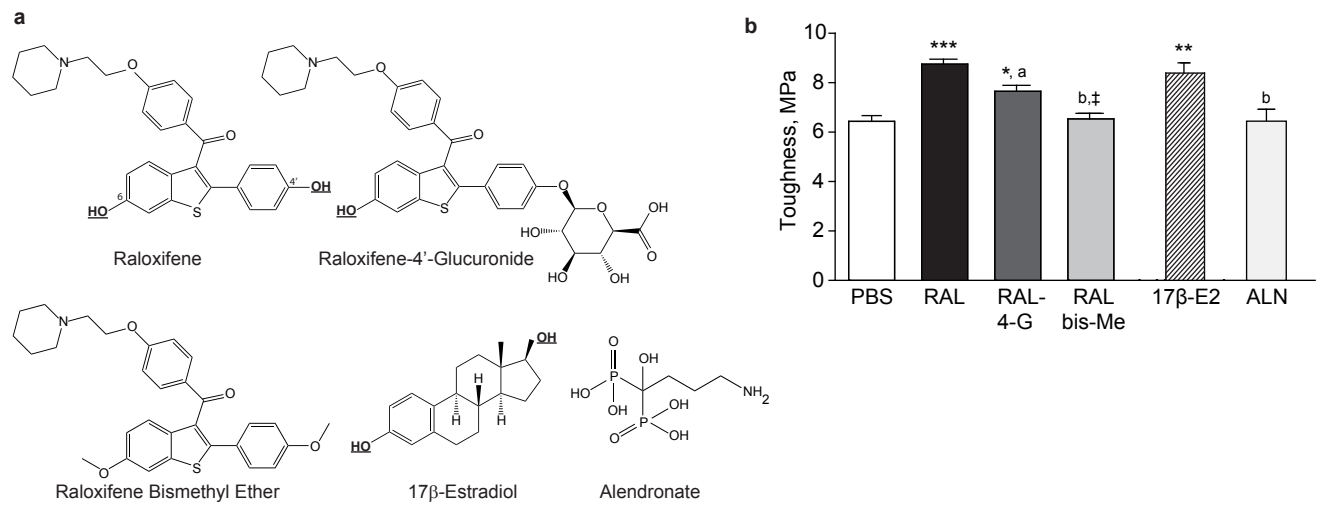


Figure 4. Gallant et al, 2013

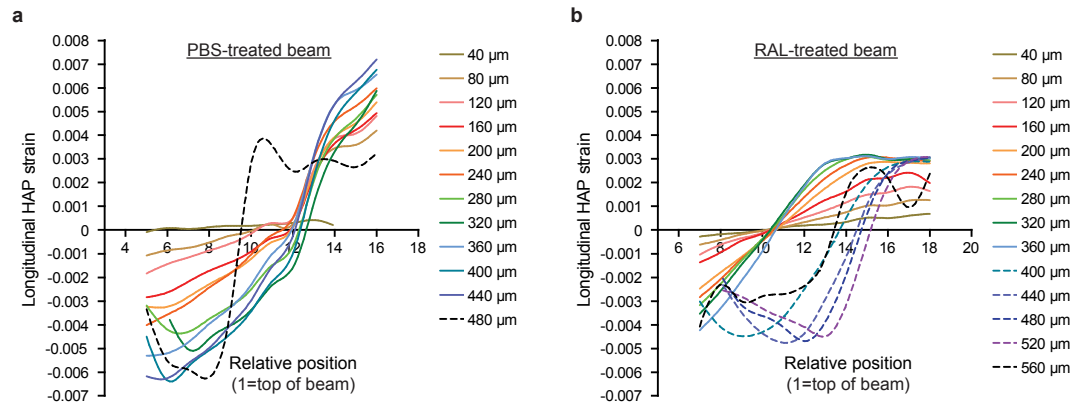


Figure 5. Gallant et al, 2013

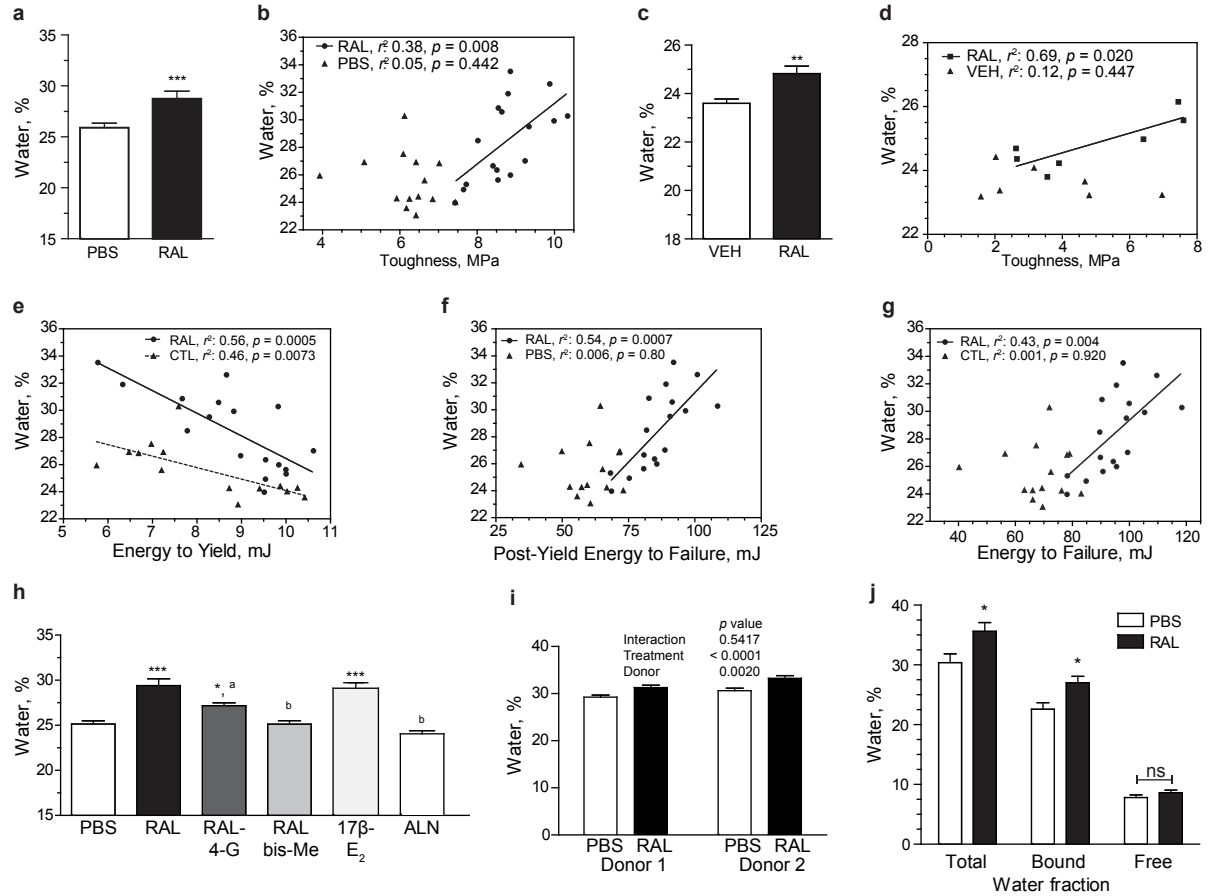
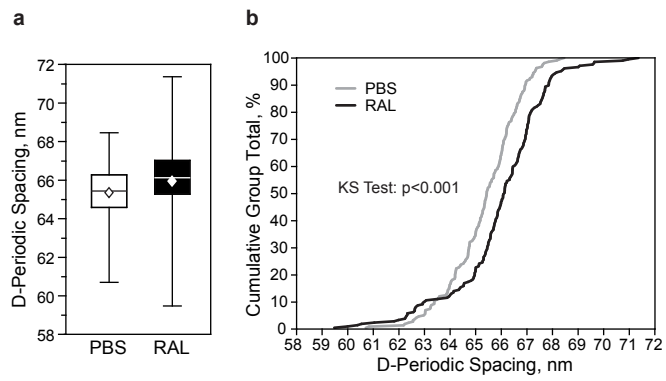
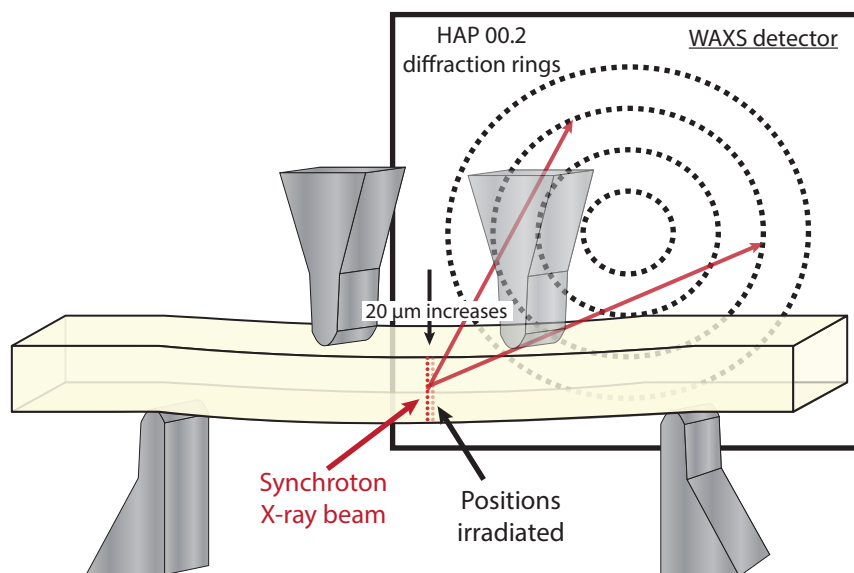


Figure 6. Gallant et al, 2013





**Supplementary Figure 1.**

## ***Supplementary Methods***

### *Lactate dehydrogenase staining:*

Canine cortical bone samples (fresh and frozen/thawed) were cut into thick sections using a diamond-coated wire saw under PBS irrigation, and polished to 100  $\mu\text{m}$ . Sections were decalcified in cold 10% EDTA in Tris buffer (0.1 M, pH 7.0) for 24 hrs. Sections were rinsed in 0.1M Tris-HCl buffer to remove/neutralize EDTA followed by 4 hrs incubation in LDH staining solution: 50 mM lithium lactate, 10 mM potassium cyanide, 5 mM magnesium chloride anhydrous, 0.6 mM NBT and 10 mM  $\beta$ -NAD in 2.5 mM phosphate buffer (pH 7.2). Sections were then fixed in 10% formol-buffered saline for 10 min, dehydrated in a graded series of EtOH (35%, 70%, 95%, 100%; 5 min each), cleared (ethanol:xylene (1:1), xylene; 5 min each) and mounted in Eukitt. Slides were analyzed under bright field microscopy.

### *DEXA*

BMD measurements were obtained by DEXA using a PIXImus densitometer (G.E. Medical Systems, Lunar Division). Each beam was scanned twice and BMD and BMC were averaged. Daily calibrations were performed using a known density phantom.

### *microCT:*

A subset of canine cortical beams were scanned (after incubation and mechanical testing,  $n=8$  per groups) with a high-resolution  $\mu\text{CT}$  system (Skyscan 1172, Belgium) using 65 kV and 120  $\mu\text{A}$  and  $0.7^\circ$  rotation steps, and then isotropic volume elements were reconstructed at 6  $\mu\text{m}$  resolution. The scanning region was defined as a 5.5 mm region located 4 mm distal of the fracture site. Scans were reconstructed and analyzed using NRecon and CTAn, respectively (Skyscan). Outcome parameters from the 3D analyses included beam bone volume (BV,  $\text{mm}^3$ ), and porosity (%).

### *RAMAN Spectroscopy:*

Raman spectral analysis was performed using a LabRAM HR 800 Raman Spectrometer (HORIBA Jobin Yvon, Edison, NJ) connected to a BX41 microscope (Olympus, Tokyo, Japan). A 633 nm He-Ne laser was focused just below the surface of the sample using the 50X objective to a spot size of  $\sim 10 \mu\text{m}$ . Five twenty second acquisitions were averaged to produce a single spectrum at each location. LabSpec 5 (HORIBA Jobin Yvon) was used to apply a five point linear baseline correction, fit a mixed Gaussian-Lorentzian function, and produce the location, height, area, and full width half maxima (FWHM) of the

$\text{PO}_4^{3-}$  -  $\nu_1$ ,  $\text{CO}_3^{2-}$  -  $\nu_1$ , and Amide I peaks. The Amide I peak was further resolved into sub peaks at  $\sim 1,660$   $\text{cm}^{-1}$  and  $\sim 1,690$   $\text{cm}^{-1}$  whose areas were obtained from the fitted curve. The mineralization, carbonate Type B substitution, and collagen crosslinking ratios were calculated by the areas of  $\text{PO}_4^{3-}$  -  $\nu_1$ / Amide I,  $\text{CO}_3^{2-}$  -  $\nu_1$ /  $\text{PO}_4^{3-}$  -  $\nu_1$ , and  $1,660$   $\text{cm}^{-1}$ /  $1,690$   $\text{cm}^{-1}$ , respectively. The crystalline maturity was found by  $1/\text{FWHM}$   $\text{PO}_4^{3-}$  -  $\nu_1$ . Each parameter was calculated at five locations approximately  $200$   $\mu\text{m}$  apart and averaged to produce the value for the sample used in the statistical analysis. A two-way t-test between the raloxifene and PBS groups was performed. Statistical analyses were carried out in SAS (Chicago, IL).

**Supplementary Table 1:** Beams size, architecture and composition.

|  | PBS     |   |       | Raloxifene |   |       | <i>p-value</i> |
|--|---------|---|-------|------------|---|-------|----------------|
|  | Mean    | ± | SD    | Mean       | ± | SD    |                |
| <b><u>Beam size</u></b>                |         |   |       |            |   |       |                |
| Canine, Thickness, mm                  | 1.37    | ± | 0.04  | 1.37       | ± | 0.02  | 0.885          |
| Canine, Width, mm                      | 2.00    | ± | 0.05  | 1.98       | ± | 0.05  | 0.221          |
| Human, Thickness, mm                   | 1.37    | ± | 0.01  | 1.37       | ± | 0.02  | 0.785          |
| Human, Width, mm                       | 2.02    | ± | 0.04  | 2.02       | ± | 0.05  | 0.882          |
| Canine Bone Density, g/cm <sup>3</sup> | 1.920   | ± | 0.020 | 1.921      | ± | 0.018 | 0.936          |
| <b><u>μCT</u></b>                      |         |   |       |            |   |       |                |
| Bone volume, mm <sup>3</sup>           | 15.45   | ± | 1.01  | 15.54      | ± | 0.60  | 0.883          |
| Total porosity, %                      | 0.395   | ± | 0.198 | 0.427      | ± | 0.184 | 0.822          |
| <b><u>RAMAN spectroscopy</u></b>       |         |   |       |            |   |       |                |
| Mineral:Matrix                         | 0.946   | ± | 0.379 | 1.367      | ± | 0.495 | 0.307          |
| Carbonate:Phosphate (Type B)           | 0.611   | ± | 0.123 | 0.495      | ± | 0.024 | 0.186          |
| Crystallinity/Maturity                 | 0.053   | ± | 0.002 | 0.056      | ± | 0.001 | 0.156          |
| Collagen Crosslinking Ratio            | 2.016   | ± | 0.161 | 1.905      | ± | 0.325 | 0.624          |
| PO <sub>4</sub> <sup>3-</sup> ν1       | 959.9   | ± | 0.6   | 960.3      | ± | 1.3   | 0.596          |
| CO <sub>3</sub> <sup>2-</sup> ν1       | 1,070.3 | ± | 1.4   | 1,069.8    | ± | 3.1   | 0.799          |
| Amide I                                | 1,677.7 | ± | 6.0   | 1,671.0    | ± | 3.7   | 0.175          |

**Supplementary Table 2:** Material properties of the experimental groups tested.

|                                | Ultimate Stress,<br>MPa |   | Elastic Modulus,<br>MPa | Toughness,<br>MPa |       | Post-Yield<br>Toughness,<br>MPa |      |
|--------------------------------|-------------------------|---|-------------------------|-------------------|-------|---------------------------------|------|
| PBS (DMSO)                     | 244.3 ± 24.6            |   | 26.2 ± 2.4              | 6.25 ± 0.85       |       | 5.69 ± 0.90                     |      |
| Raloxifene                     | 268.6 ± 24.2            | * | 27.7 ± 3.8              | 8.75 ± 0.82       | ***   | 7.94 ± 0.85                     | ***  |
| Raloxifene-4'-Glucuronate      | 248.6 ± 21.7            | a | 25.6 ± 2.8              | 7.65 ± 0.62       | **, a | 6.79 ± 0.61                     | *, a |
| Raloxifene Bismethyl Ether     | 225.8 ± 6.3             | b | 25.8 ± 2.5              | 6.54 ± 0.59       | c     | 5.92 ± 0.59                     | c    |
| Raloxifene 2 days; PBS 12 days | 247.9 ± 32.0            |   | 28.2 ± 3.4              | 8.02 ± 1.07       | **    | 7.30 ± 1.02                     | **   |
| 17β-Estradiol                  | 257.5 ± 26.7            | * | 27.8 ± 3.4              | 8.42 ± 1.16       | ***   | 7.68 ± 1.06                     | ***  |
| Donor 1: PBS (DMSO)            | 232.2 ± 8.8             |   | 26.3 ± 1.6              | 4.51 ± 1.02       |       | 3.78 ± 1.07                     |      |
| Donor 1: Raloxifene            | 226.1 ± 14.5            |   | 26.4 ± 2.3              | 5.48 ± 0.79       | *     | 4.82 ± 0.80                     | *    |
| Donor 2: PBS (DMSO)            | 219.9 ± 22.7            |   | 24.9 ± 4.0              | 5.18 ± 1.12       |       | 4.57 ± 1.08                     |      |
| Donor 2: Raloxifene            | 225.0 ± 33.8            |   | 25.4 ± 4.5              | 6.39 ± 0.81       | *     | 5.80 ± 0.79                     | *    |

\*: p<0.05, \*\*: p<0.01, \*\*\*: p<0.001 compared to PBS, a: p<0.05, b: p<0.01, c: p<0.001 compared to RAL. Data as mean ± SD.

**Supplementary Table 3:** Measured water in the raloxifene human beam group correlates with material toughness and post-yield toughness. Significant correlations are bold, and *p* values for trend (0.05 < *p* < 0.1) are indicated. Italic coefficients represent negative correlations.

|                    | Energy to Yield       |         | Energy to Failure     |               | Post-Yield Energy to Failure |               | Ultimate Stress       |              | Elastic Modulus       |         | Toughness             |               | Post-Yield Toughness  |               |
|--------------------|-----------------------|---------|-----------------------|---------------|------------------------------|---------------|-----------------------|--------------|-----------------------|---------|-----------------------|---------------|-----------------------|---------------|
|                    | <i>r</i> <sup>2</sup> | p value | <i>r</i> <sup>2</sup> | p value       | <i>r</i> <sup>2</sup>        | p value       | <i>r</i> <sup>2</sup> | p value      | <i>r</i> <sup>2</sup> | p value | <i>r</i> <sup>2</sup> | p value       | <i>r</i> <sup>2</sup> | p value       |
| All PBS (DMSO)     | 0.05                  | ns      | 0.05                  | ns            | 0.06                         | ns            | 0.05                  | ns           | 0                     | ns      | 0.07                  | ns            | 0.07                  | ns            |
| All Raloxifene     | 0.02                  | ns      | 0.53                  | <b>0.0004</b> | 0.52                         | <b>0.0005</b> | 0.26                  | <b>0.027</b> | 0.11                  | ns      | 0.59                  | <b>0.0001</b> | 0.57                  | <b>0.0002</b> |
| Donor 1 PBS        | 0.02                  | ns      | 0.32                  | 0.068         | 0.31                         | 0.072         | 0.13                  | ns           | 0.19                  | ns      | 0.36                  | 0.051         | 0.34                  | 0.058         |
| Donor 1 Raloxifene | 0.27                  | ns      | 0.36                  | <b>0.049</b>  | 0.38                         | <b>0.043</b>  | 0.25                  | ns           | 0.11                  | ns      | 0.43                  | <b>0.029</b>  | 0.44                  | <b>0.027</b>  |
| Donor 2 PBS        | 0.06                  | ns      | 0.38                  | ns            | 0.39                         | ns            | 0                     | ns           | 0.35                  | ns      | 0.37                  | ns            | 0.38                  | ns            |
| Donor 2 Raloxifene | 0.39                  | 0.096   | 0.58                  | <b>0.028</b>  | 0.51                         | <b>0.049</b>  | 0.61                  | <b>0.021</b> | 0.45                  | 0.065   | 0.63                  | <b>0.019</b>  | 0.54                  | <b>0.038</b>  |



### **Supplementary Figure Legend**

**Suppl. Fig 1.** Schematic representation of the experimental setup used during the WAXS testing. WAXS patterns are recorded for different points along the loading axis of the beam for each 20  $\mu\text{m}$  increase in displacement until sample failure. The sample was translated between displacements to minimize local x-ray dose.